ACS Catalysis

Research Article

pubs.acs.org/acscatalysis

RuPd Alloy Nanoparticles Supported on N-Doped Carbon as an Efficient and Stable Catalyst for Benzoic Acid Hydrogenation

Minghui Tang, Shanjun Mao, Mingming Li, Zhongzhe Wei, Fan Xu, Haoran Li, and Yong Wang*

Advanced Materials and Catalysis Group, ZJU-NHU United R&D Center, Department of Chemistry, Zhejiang University, Hangzhou 310028, People's Republic of China

Supporting Information

ABSTRACT: RuPd alloy nanoparticles (3.6 nm) uniformly dispersed on N-doped carbon (RuPd/CN) was prepared via a simple ultrasound-assisted coreduction method. The RuPd/CN is highly active, selective, and stable in the hydrogenation of benzoic acid to cyclohexanecarboxylic acid under mild conditions with a TOF up to 2066 h^{-1}. It was found that the bimetallic RuPd/CN catalyst exhibited a substantially enhanced activity in comparison with the monometallic catalysts (Ru/CN and Pd/CN). The reason for the higher performance of the RuPd/CN catalyst is considered to be the increased Ru^0 /Ru^{n+} ratio induced by the electronic interaction between Ru and Pd, as evidenced by various characterizations. Notably, the different phenomenon of activity platform on different catalysts ascribed to the effect of hydrogen pressure was newly observed and further explained by first-principle studies. Moreover, the factors influencing the adsorption modes of BA, especially the configuration of the carboxyl group, have been investigated preliminarily in first-principle studies, giving a distinct insight from the former work. The reason the carboxyl group in benzoic acid does not undergo hydrogenation, which results in superior selectivity (>99%), is also revealed by a comparison of the thermodynamics of hydrogenation and dissociation of the carboxyl group.

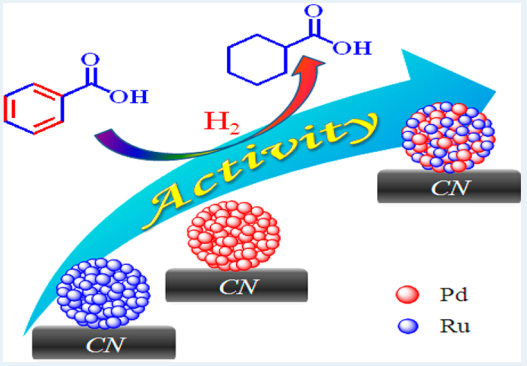

KEYWORDS: *bimetallic catalyst, RuPd alloy, N-doped carbon, chemoselective hydrogenation, benzoic acid*

1. INTRODUCTION

Cyclohexanecarboxylic acid (CCA) is an important organic intermediate for the synthesis of pharmaceuticals, such as praziquantel, hexanolactam, and ansatrienin.[1] Chemoselective hydrogenation of benzoic acid (BA) is the most effective method to obtain CCA (Scheme 1).[2] However, aromatic ring hydrogenation requires conditions more severe than those required to hydrogenate other functional groups (typically, C═O, C═C, C═N, etc.) due to the need to overcome the high resonance energy of the benzene ring.[3]

Scheme 1. Products from Divergent Pathways of Hydrogenation of BA

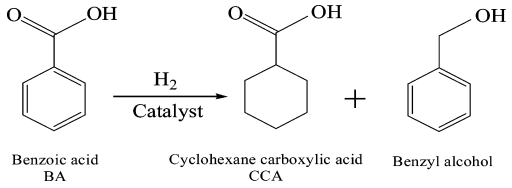

Traditionally, hydrogenation of BA has been carried out by using stoichiometric Na−K alloys.[4] It also has been found that CCA can be produced from hydrogenation of molten BA without any solvent over carbon-supported precious metal catalysts. Unfortunately, the reaction was usually carried out in $scCO_2$ or under high H_2 pressures (10−15 MPa) and high temperatures (150−200 °C).[5] Thus, preparing a high-performance and environmentally friendly catalyst that can be used under mild reaction conditions for the chemoselective hydrogenation of BA is urgently needed.

In recent years, researchers have found that Pd can be used for selective hydrogenation reactions. The activity of Pd catalysts can be controlled by varying the support materials (MgO,[6] Al_2O_3,[7] activated carbon,[8] TiO_2,[9] MCM-41,[10] mpg-C_3N_4, etc.[11−14]). As carbon materials are mainly composed of carbon and even can be made directly out of biomass, they are obviously "sustainable" support materials for Pd nanoparticles (NPs).[15] However, as reported by Anderson, the carbon-supported Pd catalyst also presented a poor activity toward aromatic ring hydrogenation; the activated carbon supported Pd (Pd/AC) converted only 34% BA to CCA after 24 h using 1 bar of hydrogen at 85 °C.[16] Furthermore, Pd deposited on carbons easily leaches during catalytic processes because the interaction between the metal and the carbon surface is weak. As a consequence, the chemical or catalytic properties of carbons do not always satisfy the sharply increasing demands of catalysis. Recent fast-growing research has been carried out on

Received: January 9, 2015
Revised: April 9, 2015
Published: April 14, 2015

DOI: 10.1021/acscatal.5b00037
ACS Catal. 2015, 5, 3100−3107

porous carbon materials, especially nitrogen-doped carbon, which has enhanced chemical, electrical, and functional properties and has been demonstrated as a novel support for heterogeneous catalysis.[17−24]

Indeed, we showed earlier that Pd NPs supported on N-doped carbon (Pd/CN) catalyzed BA hydrogenation efficiently, giving a 100% yield of CCA at 85 °C under 1 bar of H_2 pressure after 24 h.[25] However, the high price of noble-metal catalysts has limited their further application in industry. Therefore, it is desirable to find a suitable substitute for Pd having lower cost but comparable activity for BA hydrogenation. Alloying with a second metal is considered to be effective for obtaining a highly active catalyst.[26−28] In addition, the dilution of costly noble metals by inexpensive metals in bimetallic catalysts is also of interest because of the potential savings in material cost, while the catalytic performance is still maintained or even enhanced.[29−33]

Herein, considering the bimetallic effects and the advantage of lowering the cost of the catalyst, we prepared a bimetallic RuPd/CN catalyst and tested its activity in the hydrogenation of BA. We found that bimetallic catalyst RuPd/CN exhibited higher activity than the monometallic catalysts Ru/CN and Pd/CN. An obvious electronic interaction between Ru and Pd was observed through XPS, verifying the reason for the better catalytic behavior of the bimetallic catalyst in the hydrogenation reaction. The intrinsic alloy synergistic effects on the catalyst structure and catalysis behavior were investigated in depth both experimentally and theoretically. Furthermore, the as-synthesized RuPd/CN exhibits not only higher activity but also better stability toward BA hydrogenation, in comparison with Pd/CN, Ru/CN, and commercial Pd/AC catalysts.

2. RESULTS AND DISCUSSION

We have reported that Pd/CN showed higher catalytic performance in BA hydrogenation to CCA than other supported Pd catalysts (Pd/AC, Pd/metal oxide, etc.).[25] The performance of various Pd/CN catalysts modified with inexpensive metals (Ru, Cu, Fe, Ni, and In) was compared as shown in Table 1. In the bimetallic catalysts, the loading of Pd was fixed at 1 wt %; the amount of additive metal was fixed at 2.5 by the weight ratio of the additive to Pd, which is the best composition for RuPd/CN (Table S1 in the Supporting Information). Notably, RuPd/CN showed the highest BA conversion, even in comparison with Pd/CN. Unfortunately, other MPd/CN catalysts (M = Cu, Fe, Ni, and In) all showed very poor activity. Furthermore, the performance of various metal (Cu, Fe, Ni, and In) modified Ru/CN catalysts was also compared. As might be expected, RuPd/CN showed the highest BA conversion, but other RuM/CN species (M = In, Fe, Cu, Ni) showed relatively poor activity. From a catalytic point of view, the RuPd/CN catalyst already appears as quite a unique and interesting material. Next, a series of characterizations and activity tests accompanied by theoretical calculations was carried out to explain the experimental results and find the relationship between bimetallic catalyst intrinsic alloy synergistic effects and catalytic properties.

Table 1. Comparison of the Catalytic Performances in the BA Hydrogenation over Modified Pd/CN (1 wt % Pd, Secondary Metal/Pd = 2.5) and Modified Ru/CN (1 wt % M, M/Pd = 2.5)[a]

entry	catalyst	conversion, % (selectivity, %)
1	Pd/CN	38 (100)
2	CuPd/CN	0
3	FePd/CN	0
4	NiPd/CN	0
5	InPd/CN	0
6	RuPd/CN	67 (100)
7	Ru/CN	9 (100)
8	RuIn/CN	0.2 (100)
9	RuFe/CN	10 (100)
10	RuNi/CN	11 (100)
11	RuCu/CN	4 (100)

[a]Reaction conditions: BA 0.5 mmol, catalyst 50 mg, solvent water 25 mL, 85 °C, 0.1 MPa H_2, 6 h.

In order to highlight the advantage of N-doped carbon as support, a variety of non-nitrogen carbon (non-nitrogen hydrothermal carbon, HC; commercial active carbon, AC; commercial multiwall carbon nanotubes, CNT) have been used to compare with CN under identical conditions (Table 2). The textural properties of the different catalysts are given in Table S2 in the Supporting Information. Among the different catalysts, RuPd/CN was found to give the most active system (Table 2, entry 1). To clarify, the HC (from glucose) was prepared using the same method as for CN (D-glucosamine hydrochloride). RuPd/HC resulted in a BA conversion of only 28%, meaning the N atoms in RuPd/CN are of crucial importance to the catalytic activity. Thus, N-doped carbon materials as high-performance catalyst supports have great promise in heterogeneous catalysis.

Table 2. Catalytic Results for Different Catalysts[a]

entry	catalyst	conversion, % (selectivity, %)
1	RuPd/CN	67 (100)
2	RuPd/HC	28 (100)
3	RuPd/AC	45 (100)
4	RuPd/CNT	39 (100)

[a]Reaction conditions: BA 0.5 mmol, catalyst 50 mg, solvent water 25 mL, 85 °C, 0.1 MPa H_2, 6 h.

The mesoporous structure of the support and various catalysts were identified by nitrogen adsorption/desorption isotherms (Figure S4 and Table S2 in the Supporting Information). The results clearly show the support CN retained its mesoporosity well after the loading of monometallic or bimetallic nanoparticles, indicating that the CN was an excellent support.

To better understand the catalytic properties of supported bimetallic catalysts, it is necessary to explore both the distribution and the chemical states of the metals within the individual NPs. The dispersion and the average metal particle size of the RuPd/CN were confirmed by HRTEM (Figure 1). It revealed that the NPs were uniformly dispersed on the support; no significant aggregations were observed, which may result from the excellent anchoring of the CN toward the deposited NPs due to the electronegative nitrogen in the carbon structure.[15] For Pd/CN, the metal particles had an average size of 4.6 nm with a range of 2−8 nm (Figure S5 in the Supporting Information), while RuPd/CN exhibited a smaller particle size (3.6 nm) and a relatively narrow particle size distribution (2−5 nm), indicating that the introduction of Ru could effectively improve the Pd dispersion. Figure 1C shows that the particles were highly faceted. The nanocrystal plane

DOI: 10.1021/acscatal.5b00037
ACS Catal. 2015, 5, 3100−3107

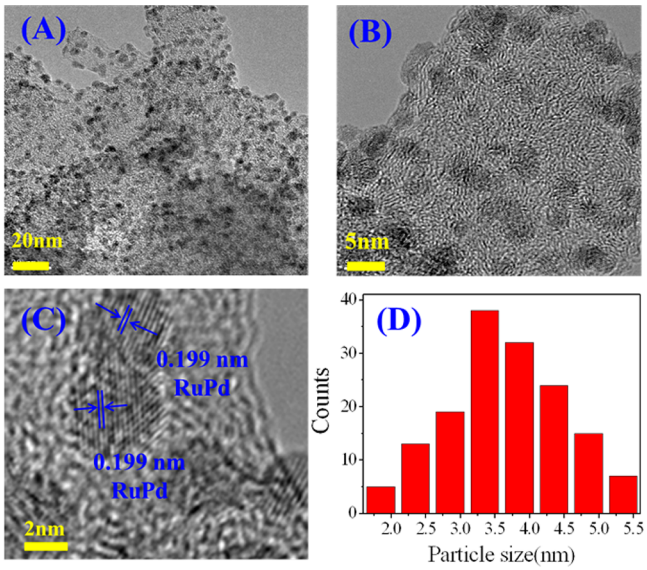

Figure 1. HRTEM images (A–C) and particle size distribution (D) of RuPd/CN.

spacing was measured as 0.199 nm, which is located between the Ru (111) value of 0.129 nm and the Pd (111) value of 0.224 nm. Furthermore, no separated Ru or Pd lattice was detected, which demonstrated that Ru and Pd distributed homogeneously in the particles of RuPd/CN.

In addition, STEM analysis was performed to clarify the structural and compositional details of RuPd NPs (Figure 2). The color distribution in HAADF images showed that the Ru and Pd X-ray signals completely homogeneous cover the spatial area of the NPs, suggesting that the alloy has been formed. EDX line scanning analysis of two optionally neighbored RuPd NPs further verified the formation of atomic-level RuPd alloy.

The XRD patterns of various samples are shown in Figure 3. All samples present a broadened peak centered at 43.2°, which could be assigned to the CN support. Diffraction peaks of Pd/CN at 2θ of 40.1, 46.7, and 68.1° are indexed to the (111), (200), and (220) crystal planes of Pd, respectively. These peaks indicate that the deposited Pd of the Pd/CN catalyst has a face-centered cubic (fcc) structure.[34] However, no characteristic

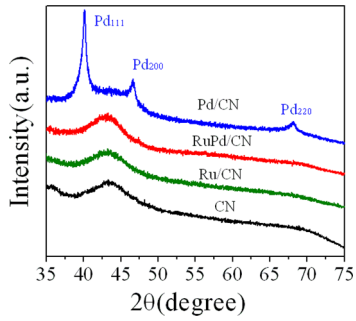

Figure 3. XRD patterns of different catalysts.

peaks of Ru can be fitted in the XRD patterns of Ru/CN, indicating that the Ru NPs are less than 4 nm in size and are well dispersed on the support, which is also in agreement with the HRTEM results (Figure S6 in the Supporting Information).[35] Moreover, no peaks corresponding to Ru and Pd are detected in the RuPd/CN catalysts, which demonstrate that the Ru and Pd form a RuPd alloy with very small particle size along with a good dispersion on the support, which is also in accordance with the HRTEM results.

To get further insight into the interactions between Ru and Pd, XPS investigations were then conducted (Figure 4). The binding energies are corrected with reference to the C 1s line at 284.5 eV. As shown in Figure 4A, an obvious positive shift (0.2–0.5 eV) in binding energy can be observed for RuPd/CN with respect to Pd/CN, indicating a change in the electronic properties of Pd caused by the alloying effect between Ru and Pd, which can be also certified by the binding energy shift of Ru. As the Ru $3d_{3/2}$ peak overlaps with that of C 1s on support CN, Ru 3p peaks are employed for all samples to determine the chemical state of Ru.[36−38] In comparison with Ru/CN, the binding energy of Ru $3p_{3/2}$ for RuPd/CN presented a negative shift (0.2–0.3 eV) after the formation of RuPd alloy.

For a more detailed understanding of the XPS measurements, Table 3 summarized the XPS-derived ratios of oxidized and reduced metal states with different catalysts, giving evidence of the surface Pd electronic state changes induced by the addition of Ru. It was found that, in contrast to monometallic catalysts (Pd/CN and Ru/CN), the ratio of Pd^0/

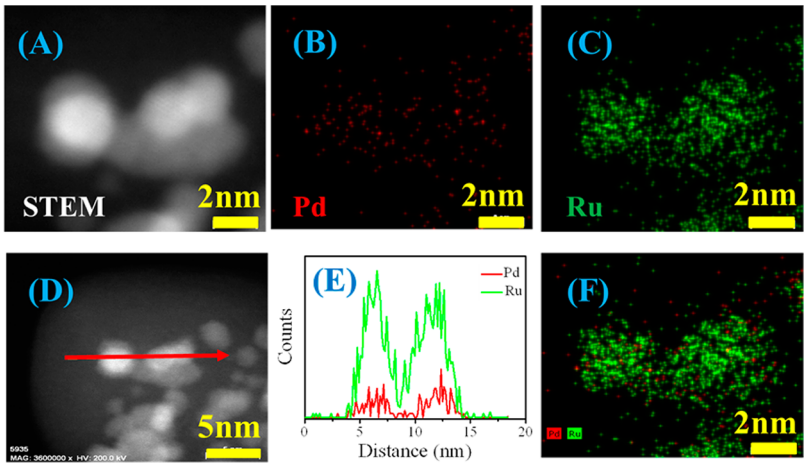

Figure 2. (A) HAADF-STEM image. (B) Pd–L and (C) Ru–L STEM-EDX maps obtained from a group of RuPd NPs of RuPd/CN. (F) Reconstructed overlay images of the maps shown in panels B and C: red, Pd; green, Ru. (E) Compositional line profiles of Pd and Ru for the RuPd NPs recorded along the arrow shown in the STEM image (D).

DOI: 10.1021/acscatal.5b00037
ACS Catal. 2015, 5, 3100–3107

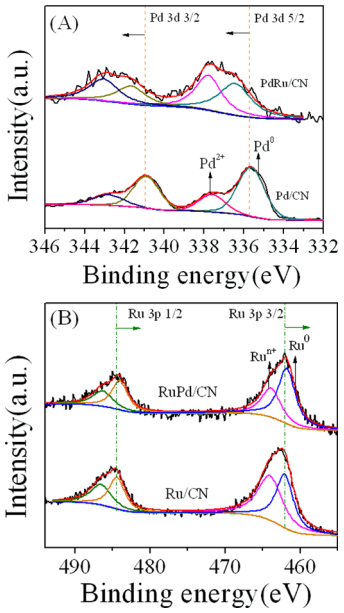

Figure 4. XPS spectra of Pd 3d (A) and Ru 3p (B) in the different catalysts.

Table 3. Binding Energies (eV) and Curve-Fitting Results of Pd 3d and Ru 3p XPS Spectra

	Pd $3d_{5/2}$, eV		Ru $3p_{3/2}$, eV		relative percentage, %	
catalyst	Pd^{2+}	Pd^{0}	Ru^{n+}	Ru^{0}	Pd^{0}/Pd^{2+}	Ru^{0}/Ru^{n+}
Pd/CN	337.6	335.6			72/28	
RuPd/CN	337.8	336.1	463.8	461.8	52/49	62/38
Ru/CN			464.0	462.1		48/52

Pd^{2+} decreased while the ratio of Ru^{0}/Ru^{n+} increased for the bimetallic catalyst (RuPd/CN), confirming that the existence of Pd promoted the reduction of Ru^{n+}. In conclusion, such shifts suggest that the electronic status of Ru and Pd was modulated as a result of alloy formation, thereby influencing the catalytic behavior of Pd in the hydrogenation reaction. This will be further confirmed by the catalyst evaluation results described below.

H_2-TPR experiments have been performed to further confirm the interaction between Ru and Pd (Figure 5). Pd/CN presents a single large hydrogen release peak centered at 70 °C, which is caused by the decomposition of palladium hydride (PdH_x), indicating the easy reducibility of Pd^{2+}.[16,31,39] However, the reduction profile of the Ru/CN catalyst shows

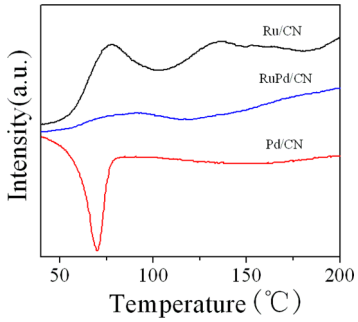

Figure 5. H_2-TPR patterns of CN-supported Pd, Ru, and RuPd catalysts.

two hydrogen consumption peaks with maxima at about 78 and 134 °C, demonstrating that two types of ruthenium oxides might have been formed on the Ru/CN catalyst.[40] For the bimetallic catalyst RuPd/CN, only a weak and broad hydrogen consumption peak in the temperature range 60−117 °C was observed, revealing that interaction occurred between Ru and Pd. We deduce that this peak may be related to the reduction of Ru oxides. Thus, the existence of Pd metal helps the reduction of ruthenium oxides, in agreement with the XPS analysis.

Having proved the successfully preparation of RuPd/CN catalyst with Ru and Pd finely alloyed together with small size, the catalytic performances were then tested in the hydrogenation of BA to CCA. As shown in Table 4, under the given

Table 4. BA Hydrogenation with Different Catalysts[a]

entry	catalyst	conversion, % (selectivity, %)	TOF_{Pd} (h^{-1})[b]
1	Pd/CN	38 (100)	1.7
2	Ru/CN	9 (100)	
3	RuPd/CN	67 (100)	11.5
4[c]	RuPd/CN	100 (100)	2066
5[d]	RûPd/CN	52 (100)	8.9

[a]Reaction conditions unless stated otherwise: BA 0.5 mmol, catalyst 50 mg, solvent water 25 mL, 85 °C, 0.1 MPa H_2, 6 h. [b]Obtained by assuming that the Pd atoms were solely responsible for the activity. [c]Reaction conditions: BA 10 mmol, catalyst 25 mg, solvent water 50 mL, 100 °C, 5 MPa H_2, 2 h. [d]This catalyst was prepared by an ultrasound-assisted two-step reduction method (see the Supporting Information).

mild reaction conditions, both Ru/CN and Pd/CN showed low BA conversion, whereas RuPd/CN exhibited a relatively high conversion of 67%. Indeed, this phenomenon results from the remarkable promotion effect of RuPd alloy formation. We also prepared RûPd/CN through an ultrasound-assisted two-step reduction method (see the Supporting Information), which also presented a lower catalytic performance in comparison with the RuPd/CN prepared by a coreduction method (Table 4, entry 5), suggesting the synergistic effect of Ru and Pd generated during the process of preparation. Consequently, the highly efficient catalytic performance of RuPd/CN inspired us to perform the scale-up experiment (Table 4, entry 4). In this typical process, BA can almost completely selectively hydrogenate to CCA within 2 h, achieving a relatively high turnover frequency (TOF) of 2066 h^{-1}.

The effects of hydrogen pressure on the activities of different catalysts were investigated as shown in Figure 6A. Interestingly, the activities of RuPd/CN and Ru/CN both increased along with the elevated pressure, while an activity platform of Ru/CN emerges at 0.8 MPa of H_2 pressure. Pd/CN shows the lowest activity to BA hydrogenation. The increase of H_2 pressure has a rare impact on the activity of Pd/CN, since the earliest platform appeared at 0.4 MPa. In order to further understand the newly found platform phenomenon, the adsorption energies of BA on Pd, Ru, and RuPd alloy have been calculated respectively, in the hope of obtaining a preliminary explanation (the relevant adsorption modes are shown in Figure S2 in the Supporting Information). As is shown in Figure 6B, BA displays no affinity for the Pd surface with small positive adsorption energy. This indicates the low concentration of the chemisorbed BA and explains the resulting early platform on Pd/CN catalyst, since the Pd surface is mostly covered by dissociated H atoms. However, the chemisorption of BA on the other two catalysts is

DOI: 10.1021/acscatal.5b00037
ACS Catal. 2015, 5, 3100−3107

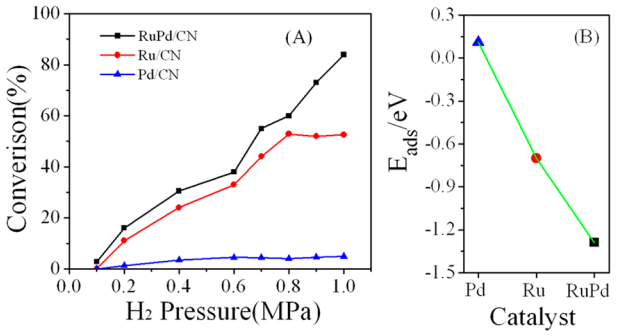

Figure 6. (A) Influence of hydrogen pressure on BA conversion with different catalysts. Reaction conditions: BA 1 mmol, catalyst 25 mg, solvent water 25 mL, 55 °C, 1 h. (B) Adsorption energies of BA on different catalysts derived from DFT calculations.

rather favorable, with adsorption energies of −0.7 and −1.29 eV for Ru and RuPd, respectively. The notable adsorption energies cause a competitive chemisorption between BA and H_2; thus, the platform for Ru/CN catalyst appears later and that for RuPd/CN catalyst never appears in the investigated H_2 pressure range due to the relatively large adsorption energy. Electronic structure analysis was then performed to determine the origin of different adsorption energies. The results showed that the electron transfer between BA and the catalysts is quite relevant to the binding strength of BA on the catalysts (see Table S4 and the related discussion in the Supporting Information for more details).

It is noteworthy that excessively large adsorption energy could lead to relatively lower activity according to the Sabatier principle.[41] The activities and adsorption energies for RuPd/CN and Ru/CN seem to be self-contradictory, due to the fact that RuPd/CN possesses a relatively larger adsorption energy, while maintaining a better activity than Ru/CN. In fact, the paradox is induced by the different amounts of active sites in different catalysts, which can be verified through XPS analysis (Table 3). In comparison with Ru/CN, the increased Ru^0/Ru^{n+} ratio in RuPd/CN occurred after the formation of RuPd alloy, which may be conducive to the enhanced activity of RuPd/CN.

Anderson[16] and Bai[42] proposed that the polar carboxyl group of BA is repulsive to the catalyst and faces upward toward a polar solvent, such as water. However, the calculation results performed here provide a distinguishing insight. When excluding the solvent is excluded, the optimized structures of the chemisorption of BA on the three catalysts reflect that the C═O of the carboxyl group (COOH) binds on the catalyst surface indeed apart from Pd (see Figure S2 in the Supporting Information). Considering the conducting experimental conditions, the adsorption modes of BA on the catalysts were recalculated by introducing the effects of solvation (see Figure 7). The adsorption mode of BA on Pd mostly remains the same, while this is not the case for Ru and RuPd catalysts. The hydrogen (H) atom in COOH dissolves in the solvent due to the ionization of water, and the two oxygen (O) atoms in reserve both bind to the surfaces of the catalysts. It can be concluded that the configuration of COOH in chemisorbed BA in water solvent is determined by both the nature of the catalysts and the effects of the solvation, through the comparison of the BA adsorption modes among the three catalysts. To be exact, the adsorption mode of the C═O fragment is in all probability affected only by the nature of the catalysts rather than the effects of the solvation, since its configuration changes little in both vacuum and water solvent on each catalyst. However, the adsorption mode of the OH fragment is likely influenced by both factors, since the H atom of COOH in vacuum dissolves in water solvent on Ru and RuPd while it remains on Pd in both cases. Unfortunately, it is hard to get the adsorption energy of BA in water solvent due to the numerous relative configurations among the water molecules. Therefore, the charge transfer is utilized as the chemisorption strength descriptor here, rather than the adsorption energy. As can be seen in Table S4 in the Supporting Information, the charge transfer of BA or the relevant acid ion changes only slightly in water solvent in comparison with that under vacuum. Thus, it is rational to deduce that the trend of the distinguishing adsorption energies of BA on different catalysts remains the same in water solvent. This is why the adsorption energies of BA on the catalysts in vacuum have been used to study the platform.

The excellent selectivity for BA hydrogenation on the three catalysts is obviously interesting. In other words, the reason the COOH group does not undergo the hydrogenation process is of great importance. Figure 7 probably can explain this in part. In water solvent, the H atom in COOH of BA which chemisorbed on Ru and RuPd catalysts respectively dissolves into water spontaneously, which means COOH of BA more likely tends to release a H atom rather than receive one. Furthermore, we calculated the respective thermodynamics of COOH dissociation and hydrogenation, under vacuum for simplicity. The energy results are shown in Table 5. For Pd, the positive COOH hydrogenation and dissociation energies, which denote endothermic reactions, imply that COOH tends to maintain itself since the surface H atoms from dissociated H_2 molecules prefer to stay on the surface rather

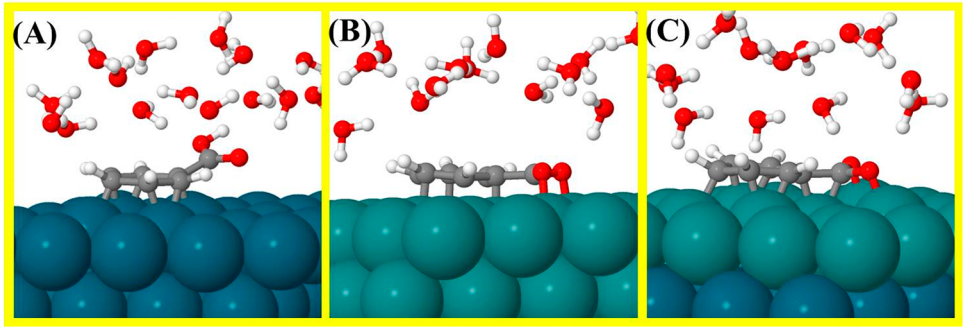

Figure 7. Optimized adsorption modes of BA in the water solvent on (A) Pd, (B) Ru, and (C) RuPd catalysts, respectively. Color code: dark green, Pd; light green, Ru; gray, C; red, O; white, H.

DOI: 10.1021/acscatal.5b00037
ACS Catal. 2015, 5, 3100−3107

Table 5. Thermodynamics of Hydrogenation and Dissociation of COOH in BA[a]

	catalyst		
	Pd	Ru	RuPd
hydrogenation	0.36	0.79	0.20
dissociation	0.65	−0.53	−0.29

[a]A negative value denotes an exothermic reaction, and a positive value denotes an endothermic reaction. The relevant optimized structures studied for COOH hydrogenation and dissociation can be seen in Figure S3 in the Supporting Information.

than bind to COOH and dissociation of COOH is thermodynamically unfavorable at low temperatures. For Ru and RuPd, the positive COOH hydrogenation and negative dissociation energies indicate that COOH thermodynamically dissociates the H atom, resulting in two O atoms binding to the catalyst surfaces. In conclusion, the hydrogenation of COOH is thermodynamically favorable in none of the cases.

Gratifyingly, RuPd/CN also showed impressive activity in the hydrogenation of benzoic acid derivatives (Table S6 in the Supporting Information). In a final set of experiments, the reusability of RuPd/CN in contrast with commercial Pd/AC (Pd loading is 5 wt %) was investigated (Figure 8). The results

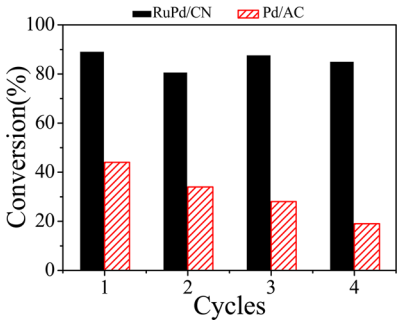

Figure 8. Comparison of the reusability of the RuPd/CN and commercial Pd/AC in the BA hydrogenation under the same reaction conditions. Reaction conditions: BA 0.75 mmol, catalyst 50 mg, solvent water 25 mL, 55 °C, 0.4 MPa H_2 pressure, 1 h.

revealed that, after easy separation and pretreatment, RuPd/CN still could achieve a high conversion of 85% after four batches, demonstrating its good deactivation resistance and recyclability. However, for commercial Pd/AC, there was a considerable decrease in catalytic activity during these recycling tests. Furthermore, no traces of leached Ru or Pd species were detected in the reaction filtrate of RuPd/CN as catalyst. These results demonstrated that the highly active RuPd/CN was more stable than commercial Pd/AC under the investigated conditions. Its excellent catalytic performance and good recyclability should make the RuPd/CN catalyst attractive for both fundamental research and practical applications.

3. CONCLUSIONS

Alloyed RuPd/CN catalyst was prepared via a simple ultrasound-assisted coreduction technique, exhibiting a remarkably superior activity and excellent stability over their monometallic counterparts for the hydrogenation of BA under mild conditions. The excellent catalytic performance was mainly attributed to the increased Ru^0/Ru^{n+} ratio induced by RuPd formation confirmed by various characterizations. The platform on the activity to the H_2 pressure presenting different phenomena on different catalysts was further explained by calculating the adsorption energy of BA on the catalysts from a first-principle view. The unique phenomenon was due to the relatively strong adsorption energies of BA on RuPd/CN. The factors influencing the adsorption modes of BA, especially the configuration of the carboxyl group, were investigated preliminarily by first-principle studies, giving a distinct view from the former work. The reason the carboxyl group in BA does not undergo hydrogenation, which results in superior selectivity (>99%), is also revealed by comparisons of the thermodynamics of hydrogenation and dissociation of the carboxyl group. In addition, the strategy reported here provides a means for seeking more economical metal elements alloying with noble metal to prepare bimetallic catalysts, which are applicable to various hydrogenation reactions, with superior catalytic performance.

4. EXPERIMENTAL SECTION

4.1. Catalyst Preparation. The N-doped carbon (CN) was synthesized as described previously.[25] Bimetallic MPd/CN (M = Ru, Cu, Fe, Ni, In) and RuM/CN (M = Cu, Fe, Ni, In) catalysts were prepared by ultrasound-assisted coreduction methods. With the typical synthesis of RuPd/CN as an example, appropriate amounts of CN were dispersed in deionized water in a beaker under ultrasound, and then the desired amounts of $RuCl_3$ aqueous solution (0.01 g/mL) and Na_2PdCl_4 aqueous solution (0.01 g/mL) were placed in the beaker under treatment in ultrasound for 10 min. Then 10 mL of freshly prepared $NaBH_4$ aqueous solution (2 mg/mL) was added to the suspension under ultrasound treatment for another 30 min. The solid was separated from the solution by filtration and washed with water thoroughly. The obtained catalyst was dried at 70 °C overnight, and then it was treated with a simple grinding and denoted as RuPd/CN. Pd/CN and Ru/CN were prepared using the same methodology for comparison.

4.2. Catalyst Characterization. The BET specific surface areas were measured on a surface area and porosity analyzer (Micromeritics, ASAP 2020 HD88). The actual contents of Ru and Pd in the prepared catalysts were measured by inductively coupled plasma-atomic emission spectroscopy (ICP-AES) on a Plasma-Spec-II spectrometer. The dispersion of Pd was calculated on the basis of CO chemisorption at room temperature, using a CHEMBET-3000 apparatus (Quantachrome Co.). High-resolution transmission electron microscopy (HRTEM) was carried out on an FEI Tecnai G2 F20 S-TWIN microscope. High-resolution scanning transmission electron microscopy (HRSTEM) high-angle annular dark field (HAADF) STEM, and EDX analyses were recorded on a Titan G280-200 w/ChemiSTEM instrument. X-ray power diffraction analysis (XRD) was performed using an Ultima TV X-ray diffractometer with Cu Kα radiation (1.54 Å). The X-ray photoelectron spectra (XPS) were obtained by an ESCALAB MARK II spherical analyzer using an aluminum−magnesium binode (Al. 1486.6 eV; Mg, 1253.6 eV) X-ray source. Hydrogen temperature-programmed reduction (H_2-TPR) was conducted with a FINESORB-3010 apparatus equipped with a thermal conductivity detector (TCD). Before a TPR run, catalysts were pretreated in Ar at 473 K for 2 h. TPR was performed under a flow of 10% H_2/Ar gas mixture at a flow rate of 10 sccm with a temperature ramp of 10 °C/min.

DOI: 10.1021/acscatal.5b00037
ACS Catal. 2015, 5, 3100−3107

4.3. Hydrogenation of BA. In a typical process, 0.5 mmol of BA and 50 mg of RuPd/CN were placed in a three-neck flask, and 25 mL of deionized water was employed as a green solvent. The reaction was carried out at a temperature of 85 °C with magnetic stirring at a speed of 1000 rpm. Before reaction, a balloon filled with hydrogen was connected to the flask to replace the air. After the reaction, the contents of products and substrate were determined by GC-FID and the products were identified by GC-MS.

4.4. Computational Setup. The calculations reported here were performed by using periodic, spin-polarized DFT as implemented in the Vienna ab initio program package (VASP).[43,44] The electron−ion interactions have been described by the projector augmented wave (PAW) method proposed by Blöchl[45] and implemented by Kresse.[46] The RPBE functional[47] was used as an exchange-correlation functional approximation, and a plane wave basis set with an energy cutoff of 400 eV was used. Only γ point was used for the Brillouin zone sampling, during the structure optimization, while a k point of 3*3*1 was used for Bader charge analysis.[48] A p (5×5) supercell containing a 4-layer slab with 100 atoms was modeled. The periodic condition was employed along the x and y directions. The vacuum space along the z direction was set to be 13 Å. For the RuPd catalyst, Pd was alloyed to the sublayer of the Ru catalyst (Figure S1 in the Supporting Information). The upper two layer atoms in the cell were allowed to relax during the structure optimization, and the bottom two layer atoms were fixed. When solvent, i.e. water, was considered, two water layers with 17 water molecules were introduced to simulate a similar density of the liquid water phase. The relaxation was stopped when the force residue on the atom was smaller than 0.02 eV/Å. The adsorption energy for BA chemisorption is defined as

$$E_{ads} = E_{tot} - E_{slab} - E_{BA}$$

where E_{tot} is the total energy after BA adsorption on the catalysts, E_{slab} is the energy of the clean catalyst alone, and E_{BA} is the energy of BA in the gas phase.

■ ASSOCIATED CONTENT

Supporting Information

The following file is available free of charge on the ACS Publications website at DOI: 10.1021/acscatal.5b00037.

Experimental details, ICP-AES results, curve fitting of N_2 adsorption−desorption isotherms, HRTEM images of Ru/CN and Pd/CN catalysts, the effect of time and solvents on catalyst activity, and the hydrogenation of benzoic acid derivatives (PDF)

■ AUTHOR INFORMATION

Corresponding Author

*Y.W.: e-mail, chemwy@zju.edu.cn; fax, +86-571-87951895.

Notes

The authors declare no competing financial interest.

■ ACKNOWLEDGMENTS

Financial support from the National Natural Science Foundation of China (21376208), the Zhejiang Provincial Natural Science Foundation for Distinguished Young Scholars of China (LR13B030001), the Specialized Research Fund for the Doctoral Program of Higher Education (J20130060), the Fundamental Research Funds for the Central Universities, the Program for Zhejiang Leading Team of S&T Innovation, the Partner Group Program of the Zhejiang University, and the Max-Planck Society is greatly appreciated.

■ REFERENCES

(1) Moore, B. S.; Cho, H.; Casati, R.; Kennedy, E.; Reynolds, K. A.; Mocek, U.; Beale, J. M.; Floss, H. G. *J. Am. Chem. Soc.* **1993**, *115*, 5254−5266.

(2) Temkin, M.; Konyukhov, V. Y.; Kul'kova, N. *JOURNAL OF THE RESEARCH INSTITUTE FOR CATALYSIS HOKKAIDO UNIVERSITY* **1981**, *28*, 363−370.

(3) Anderson, J.; McKenna, F.-M.; Linares-Solano, A.; Wells, R. K. *Catal. Lett.* **2007**, *119*, 16−20.

(4) Gaude, D.; Le Goaller, R.; Luche, J.-L.; Pierre, J.-L. *Tetrahedron Lett.* **1984**, *25*, 5897−5898.

(5) Wang, H.; Zhao, F. *Int. J. Mol. Sci.* **2007**, *8*, 628−634.

(6) Claus, P.; Berndt, H.; Mohr, C.; Radnik, J.; Shin, E.-J.; Keane, M. A. *J. Catal.* **2000**, *192*, 88−97.

(7) Cervantes, G. G.; Aires, F. C. S.; Bertolini, J. *J. Catal.* **2003**, *214*, 26−32.

(8) Cabiac, A.; Delahay, G.; Durand, R.; Trens, P.; Coq, B.; Plée, D. *Carbon* **2007**, *45*, 3−10.

(9) Panpranot, J.; Kontapakdee, K.; Praserthdam, P. *J. Phys. Chem. B* **2006**, *110*, 8019−8024.

(10) Panpranot, J.; Pattamakomsan, K.; Goodwin, J. G., Jr; Praserthdam, P. *Catal. Commun.* **2004**, *5*, 583−590.

(11) Wang, Y.; Yao, J.; Li, H.; Su, D.; Antonietti, M. *J. Am. Chem. Soc.* **2011**, *133*, 2362−2365.

(12) Ueno, T.; Suzuki, M.; Goto, T.; Matsumoto, T.; Nagayama, K.; Watanabe, Y. *Angew. Chem.* **2004**, *116*, 2581−2584.

(13) Liu, H.; Jiang, T.; Han, B.; Liang, S.; Zhou, Y. *Science* **2009**, *326*, 1250−1252.

(14) Zhao, C.; Kou, Y.; Lemonidou, A. A.; Li, X.; Lercher, J. A. *Angew. Chem.* **2009**, *121*, 4047−4050.

(15) Xu, X.; Li, Y.; Gong, Y.; Zhang, P.; Li, H.; Wang, Y. *J. Am. Chem. Soc.* **2012**, *134*, 16987−16990.

(16) Anderson, J. A.; Athawale, A.; Imrie, F. E.; McKenna, F. M.; McCue, A.; Molyneux, D.; Power, K.; Shand, M.; Wells, R. P. K. *J. Catal.* **2010**, *270*, 9−15.

(17) Amadou, J.; Chizari, K.; Houllé, M.; Janowska, I.; Ersen, O.; Bégin, D.; Pham-Huu, C. *Catal. Today* **2008**, *138*, 62−68.

(18) Elías, A. L.; Botello-Méndez, A. s. R.; Meneses-Rodríguez, D.; Jehová González, V.; Ramírez-Gonzáalez, D.; Ci, L.; Muñoz-Sandoval, E.; Ajayan, P. M.; Terrones, H.; Terrones, M. *Nano Lett.* **2009**, *10*, 366−372.

(19) Zhang, P.; Yuan, J.; Fellinger, T.-P.; Antonietti, M.; Li, H.; Wang, Y. *Angew. Chem., Int. Ed.* **2013**, *52*, 6028−6032.

(20) Liu, R.; Mahurin, S. M.; Li, C.; Unocic, R. R.; Idrobo, J. C.; Gao, H.; Pennycook, S. J.; Dai, S. *Angew. Chem., Int. Ed.* **2011**, *50*, 6799−6802.

(21) Yang, S.; Feng, X.; Wang, X.; Müllen, K. *Angew. Chem., Int. Ed.* **2011**, *50*, 5339−5343.

(22) Yang, W.; Fellinger, T.-P.; Antonietti, M. *J. Am. Chem. Soc.* **2010**, *133*, 206−209.

(23) Fulvio, P. F.; Lee, J. S.; Mayes, R. T.; Wang, X.; Mahurin, S. M.; Dai, S. *Phys. Chem. Chem. Phys.* **2011**, *13*, 13486−13491.

(24) Lee, J. S.; Wang, X.; Luo, H.; Baker, G. A.; Dai, S. *J. Am. Chem. Soc.* **2009**, *131*, 4596−4597.

(25) Xu, X.; Tang, M.; Li, M.; Li, H.; Wang, Y. *ACS Catal.* **2014**, *4*, 3132−3135.

(26) Yang, X.; Chen, D.; Liao, S.; Song, H.; Li, Y.; Fu, Z.; Su, Y. *J. Catal.* **2012**, *291*, 36−43.

(27) Henning, A. M.; Watt, J.; Miedziak, P. J.; Cheong, S.; Santonastaso, M.; Song, M.; Takeda, Y.; Kirkland, A. I.; Taylor, S. H.; Tilley, R. D. *Angew. Chem., Int. Ed.* **2013**, *52*, 1477−1480.

(28) Hirasawa, S.; Watanabe, H.; Kizuka, T.; Nakagawa, Y.; Tomishige, K. *J. Catal.* **2013**, *300*, 205−216.

DOI: 10.1021/acscatal.5b00037
ACS Catal. 2015, 5, 3100−3107

(29) Hermannsdörfer, J.; Friedrich, M.; Miyajima, N.; Albuquerque, R. Q.; Kümmel, S.; Kempe, R. *Angew. Chem., Int. Ed.* **2012**, *51*, 11473−11477.
(30) Vicente, A.; Lafaye, G.; Especel, C.; Marécot, P.; Williams, C. T. *J. Catal.* **2011**, *283*, 133−142.
(31) Sun, J.; Karim, A. M.; Zhang, H.; Kovarik, L.; Li, X. S.; Hensley, A. J.; McEwen, J.-S.; Wang, Y. *J. Catal.* **2013**, *306*, 47−57.
(32) Lee, J.; Kim, Y. T.; Huber, G. W. *Green Chem.* **2014**, *16*, 708−718.
(33) Jin, X.; Dang, L.; Lohrman, J.; Subramaniam, B.; Ren, S.; Chaudhari, R. V. *ACS Nano* **2013**, *7*, 1309−1316.
(34) Son, S. U.; Jang, Y.; Park, J.; Na, H. B.; Park, H. M.; Yun, H. J.; Lee, J.; Hyeon, T. *J. Am. Chem. Soc.* **2004**, *126*, 5026−5027.
(35) Wang, C.; Li, B.; Lin, H.; Yuan, Y. *J. Power Sources* **2012**, *202*, 200−208.
(36) Luo, G.; Yan, S.; Qiao, M.; Zhuang, J.; Fan, K. *Appl. Catal., A* **2004**, *275*, 95−102.
(37) Kusada, K.; Kobayashi, H.; Ikeda, R.; Kubota, Y.; Takata, M.; Toh, S.; Yamamoto, T.; Matsumura, S.; Sumi, N.; Sato, K.; Nagaoka, K.; Kitagawa, H. *J. Am. Chem. Soc.* **2014**, *136*, 1864−1871.
(38) Fang, M.; Machalaba, N.; Sanchez-Delgado, R. A. *Dalton Transactions* **2011**, *40*, 10621−10632.
(39) Sá, J.; Arteaga, G. D.; Daley, R. A.; Bernardi, J.; Anderson, J. A. *J. Phys. Chem. B* **2006**, *110*, 17090−17095.
(40) da-Silva, J. W.; Cobo, A. J. G. *Appl. Catal., A* **2003**, *252*, 9−16.
(41) Knözinger, H.; Kochloefl, K. Heterogeneous Catalysis and Solid Catalysts. In *Ullmann's Encyclopedia of Industrial Chemistry*; Wiley-VCH: Weinheim, Germany, 2000.
(42) Bai, G.; Wen, X.; Zhao, Z.; Li, F.; Dong, H.; Qiu, M. *Ind. Eng. Chem. Res.* **2013**, *52*, 2266−2272.
(43) Kresse, G.; Furthmüller, J. *Comput. Mater. Sci.* **1996**, *6*, 15−50.
(44) Kresse, G.; Furthmüller, J. *Phys. Rev. B: Condens. Matter Mater. Phys.* **1996**, *54*, 11169.
(45) Blöchl, P. E. *Phys. Rev. B: Condens. Matter Mater. Phys.* **1994**, *50*, 17953.
(46) Kresse, G.; Joubert, D. *Phys. Rev. B: Condens. Matter Mater. Phys.* **1999**, *59*, 1758.
(47) Hammer, B.; Hansen, L. B.; Nørskov, J. K. *Phys. Rev. B: Condens. Matter Mater. Phys.* **1999**, *59*, 7413.
(48) Bader, R. F. W. Atoms in Molecules. In *Encyclopedia of Computational Chemistry*; Wiley: Chichester, U.K., 2002.

DOI: 10.1021/acscatal.5b00037
ACS Catal. 2015, 5, 3100−3107